Structure-antiproliferative activity studies on L-proline- and homoproline-4-*N*-pyrrolidine-3-thiosemicarbazone hybrids and their nickel(II), palladium(II) and copper(II) complexes

Aliona Dobrova,[a] Sonja Platzer,[a] Felix Bacher,[a] Miljan N. M. Milunovic,[a] Anatolie Dobrov,[a] Gabriella Sprengler,[b] Éva A. Enyedy,[c] Ghenadie Novitchi,[d] Vladimir B. Arion*,[a]

[a]*University of Vienna, Institute of Inorganic Chemistry, Währinger Strasse 42, A-1090 Vienna, Austria*

[b]*Department of Medical Microbiology and Immunobiology, University of Szeged, Dóm tér 10, H-6720 Szeged, Hungary*

[c]*Department of Inorganic and Analytical Chemistry, University of Szeged, Dóm tér 7, H-6720 Szeged, Hungary*

[d]*Laboratoire National des Champs Magnetiques Intenses-CNRS, 25 Avenue des Martyrs, 38042 Grenoble Cedex 9, France*

Nickel(II), palladium(II), copper(II), L-proline-4-*N*-pyrrolidine-thiosemicarbazone, homoproline-4-*N*-pyrrolidine-thiosemicarbazone, antiproliferative activity

Abstract

Two chiral and water-soluble thiosemicarbazone-proline (H_2L^1) and thiosemicarbazone-homoproline hybrids (H_2L^2) were synthesized. By reaction of H_2L^1 with $NiCl_2{\cdot}6H_2O$, $PdCl_2$ and $CuCl_2{\cdot}2H_2O$, in ethanol the series of square-planar complexes $[Ni(H_2L^1)Cl]Cl{\cdot}1.3H_2O$ (**1**$\cdot 1.3H_2O$), $[Pd(H_2L^1)Cl]Cl{\cdot}H_2O$ (**2**$\cdot H_2O$) and $[Cu(H_2L^1)Cl]Cl{\cdot}0.7H_2O$ (**3**$\cdot 0.7H_2O$) were prepared, while starting from H_2L^2 and $CuCl_2{\cdot}2H_2O$ in methanol the complex $[Cu(H_2L^2)Cl]Cl{\cdot}H_2O$ (**4**$\cdot H_2O$) was obtained. The compounds have been characterized by elemental analysis, spectroscopic methods (IR, UV−vis and NMR spectroscopy), ESI mass spectrometry and single crystal X-ray crystallography (H_2L^1, **1** and **2**). As a solid, **1** is diamagnetic, while paramagnetic in methanolic solution. The effective magnetic moment of 3.26 B.M. at room temperature indicates the change of coordination geometry from square-planar to octahedral after dissolution. The *in vitro* anticancer potency of ligand precursors H_2L^1 and H_2L^2 and metal complexes **1**−**4** was studied in three human cancer cell lines (A549, CH1 and SW480) an in non-cancerous fibroblasts (NIH/3T3), and the mechanism of cell death was also assayed by flow cytometry. Clear-cut structure-activity relationships have been established. The metal ions exert marked effects in a divergent manner: copper(II) increases, whereas nickel(II) and palladium(II) decrease the cytotoxicity of the hybrids. The antiproliferative activity of H_2L^1 and metal complexes **1**−**3** decreases in all three tumor cell lines in the following rank order: **3** > H_2L^1 > **1** > **2**. The role of square-planar geometry in the underlying mechanism of cytotoxicity of the metal complexes studied seems to be negligible, while structural modifications at the terminal amino group of thiosemicarbazide and proline moiety are significant for enhancing the antiproliferative activity of both hybrids and copper(II) complexes.

Introduction

α-(*N*)-Heterocyclic thiosemicarbazones (TSCs) are a class of highly potent inhibitors of ribonucleotide reductase (RNR) enzyme.[1,2] RNR catalyzes the reduction of all four ribonucleotides to their corresponding deoxyribonucleotides, and thereby provides the precursors needed for both synthesis and repair of DNA. Currently, the most studied therapeutic compound among the thiosemicarbazones is Triapine (3-aminopyridine-2-carboxaldehyde thiosemicarbazone). It is by a factor of 1000 more potent inhibitor of hR2 RNR activity than hydroxyurea, a clinically used RNR inhibitor.[3] Triapine has entered several phase II clinical trials as a chemotherapeutic agent.[4] However, this investigational drug showed severe side effects, while only little response was observed.[5,6,7,8] Another promising drug, di-2-pyridylketone 4-cyclohexyl-4-methyl-3-thiosemicarbazone (DpC) is scheduled to enter clinical trials in 2016,[9] but RNR is not or only in part responsible for its biological activity.

Many thiosemicarbazones are excellent chelators for transition metal ions, such as iron(II), copper(II) and zinc(II), typically coordinating *via* X, N, S atoms, where X is the donor atom of the additional functional group of the aldehyde or ketone used for their preparation.[10] The coordination of these TSCs can result in metal complexes with higher cytotoxicity than that of the ligand precursors. In addition, the enhanced need for the essential metal ions of cancer cells *vs* healthy cells makes the development of new chelators as anticancer agents an important task.[11,12] Copper(II) complexes are promising anticancer agents,[13] often exhibiting very high antiproliferative activity *in vitro*. In particular, copper(II) complexes with acyl diazine thiosemicarbazones bearing an *N*4-azabicyclo[3.2.2]-nonane group showed cytotoxic activity against colon adenocarcinoma HT-29 cells with IC_{50} values ranging from 0.004 to 1.51 μM and human acute lymphoblastic leukemia CCRF-CEM cells with IC_{50} values from 0.005 to 1.16 μM.[14]

Recently a series of copper(II)-TSC complexes has been tested for their topoisomerase IIα inhibition activity with the conclusion that the complexes are more potent topoisomerase IIα inhibitors compared to the corresponding ligand precursors.[15] One of such copper(II) complexes was [CuLCl], where HL = 2-pyridinealdehyde 4-*N*-ethylthiosemicarbazone. The main prerequisite for their topoisomerase IIα inhibition properties was suggested to be the square-planar coordination geometry of copper(II) in these complexes.

Despite their high cytotoxicity *in vitro*, low water solubility, high lipophilicity and high *in vivo* toxicity are the main disadvantages of TSC compounds as anticancer agents,[16] so that one of the current challenges is the design of new active TSCs and their metal complexes with enhanced aqueous solubility[17] and *a priori* oriented towards a cancer specific target.[18] We have shown that 2-hydroxybenzaldehyde thiosemicarbazone (STSC) can be coupled to L- or D-proline (Pro) leading to hybrids with enhanced aqueous solubility.[19] Although these new systems show only moderate cytotoxic potency with IC_{50} values of 62 and 75 μM, respectively, in ovarian carcinoma CH1 cells and >100 μM in colon carcinoma SW480 cells, coordination of these ligands to copper(II) resulted in 13 and 5-fold increase in cytotoxicity in CH1 cells, based on a comparison of IC_{50} values, while in SW480 cells the enhancement of the antiproliferative activity was even higher. In both tested cell lines, L-Pro-STSC as well as its copper(II) complex showed slightly stronger antiproliferative activity than the compounds with a D-Pro moiety, yielding IC_{50} values of 4.6 and 5.5 μM for [Cu(L-Pro-STSC)Cl]Cl in CH1 and SW480 cells, respectively.[19] Moreover, the preliminary data on screening the topoisomerase IIα inhibiting activity indicate that the square-planar copper(II) complexes prepared by us are indeed potential inhibitors of the topoisomerase IIα enzyme in contrast to the corresponding metal-free conjugates, which are devoid of such activity.

The quite recently reported results[19] prompted us to prepare new 2-hydroxybenzaldehyde thiosemicarbazones substituted at the terminal nitrogen atom to enhance the lipophilicity and coupled to two related α- and β-amino acid homologs, namely proline and homoproline. We anticipated that these new conjugates will form square-planar metal complexes enabling the elucidation of (i) the role of square-planar coordination geometry of the metal complexes in the underlying mechanism of antiproliferative activity, (ii) the effect of metal coordination and (iii) substitution at the terminal nitrogen atom of thiosemicarbazide moiety, as well as (iv) the effect of homologization of proline to β^3-homoproline on antiproliferative activity in cancer cell lines. Herewith we report on the synthesis of two organic conjugates, namely 5-methyl-2-hydroxybenzaldehyde 4-*N*-pyrrolidine-3-thiosemicarbazone coupled to L-proline and (*S*)-β^3-homoproline, respectively, and four new complexes with nickel(II), palladium(II) and copper(II) (Chart 1), their characterization by elemental analysis, spectroscopic methods, X-ray crystallography and antiproliferative activity in three human cancer cell lines (A549, CH1 and SW480) and in non-cancerous mouse fibroblasts (NIH/3T3). Clear-cut structure-activity relationships were established and discussed.

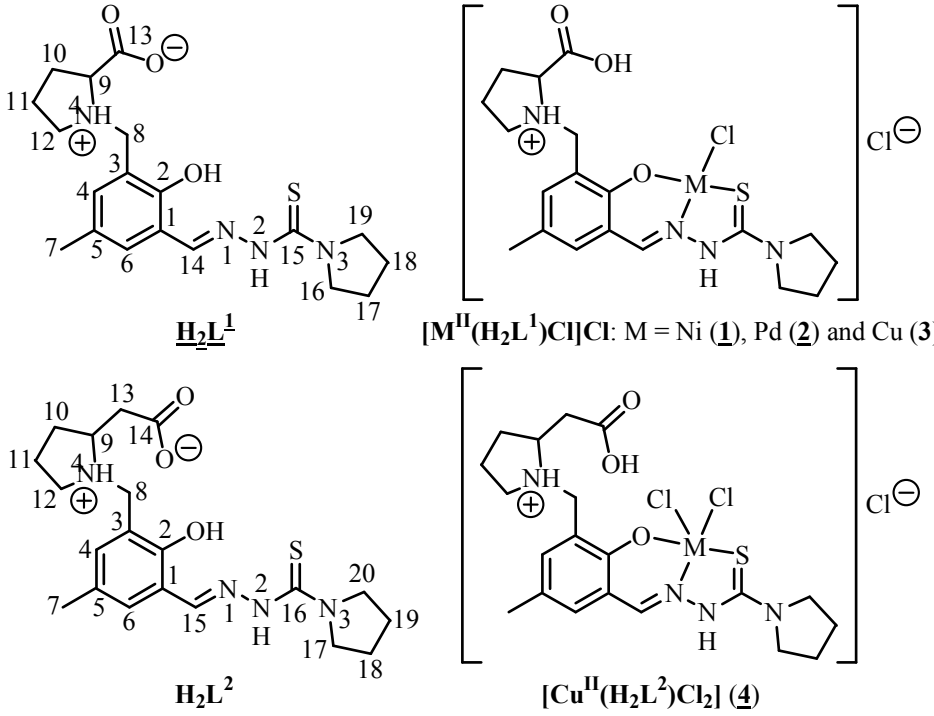

Chart 1. Line drawings of L-proline and (S)-β^3-homoproline thiosemicarbazone conjugates H_2L^1 and H_2L^2, as well as of their nickel(II), palladium(II) and copper(II) complexes. We use for consistency the same abbreviation H_2L^1 and H_2L^2 for the overall charge-neutral ligand precursors and ligands, although the charge distribution in these species is clearly different. Underlined formula and numbers indicate compounds studied by X-ray crystallography.

Experimental section

Chemicals. All reagents were used as purchased from commercial suppliers. L-Proline was from Alfa Aesar. 4-Pyrrolidine-3-thiosemicarbazide[20] was obtained in 60% yield by refluxing methyl hydrazinecarbodithioate[21] and pyrrolidine in water for 6 h. 3-Chloromethyl-2-hydroxy-5-methylbenzaldehyde was synthesized by following a modified published procedure.[22] Z-L-Proline[23] and β^3-homoproline[24] were synthesized according to previously reported protocols. All utilized solvents were HPLC grade and used without further purification.

Synthesis of Ligand Precursors

[1-(3-formyl-2-hydroxy-5-methylbenzyl)-(*R*/*S*)-pyrrolidine-2-yl]acetic acid methyl ester. To a solution of 3-chloromethyl-2-hydroxy-5-methylbenzaldehyde (0.94 g, 5.09 mmol) in THF (10 mL) was added a solution of methyl (*R*/*S*)-pyrrolidin-2-yl-acetate (0.79 g, 5.59 mmol) in methylene chloride (5 mL) followed by a solution of triethylamine (1.09 mL, 7.64 mmol) in THF (2 mL) and the reaction mixture was stirred at 60 °C for 10 h. Then THF (100 mL) was added and the crystallized triethylammonium chloride was filtered off. The orange solution was concentrated under reduced pressure and purified by column chromatography by using a 1:1 mixture ethyl acetate/hexane as eluent (R_f = 0.14). The yellow oil was dried in vacuo. Yield: 1.18 g, 80%. ^{1}H NMR (500.10 MHz, DMSO-d_6): δ 10.24 (s, 1H, HC=O), 7.36 (d, *J* = 2.0 Hz, 1H, Ar-H), 7.25 (d, *J* = 2.0 Hz, 1H, Ar-H), 4.16 (d, *J* = 14.1 Hz, 1H, Ar-C*H*$_2$-N), 3.60 (s, 3H, OCH_3), 3.54 (d, *J* = 14.2 Hz, 1H, Ar-C*H*$_2$-N), 2.98–2.91 (m, 1H, Pyrr), 2.91–2.85 (m, 1H, Pyrr), 2.81–2.74 (m, 1H, Pyrr), 2.45 (dd, *J* = 7.6 and 8.1 Hz, 2H, C*H*$_2$COOMe), 2.33–2.27 (m, 1H, Pyrr), 2.24 (s, 3H, CH_3), 2.08–2.00 (m, 1H, Pyrr), 1.76–1.67 (m, 3H, Pyrr), 1.61–1.53 (m, 1H, Pyrr) ppm. ^{13}C{1H} NMR (125.76 MHz, DMSO-d_6): δ 191.78, 172.18, 159.25, 136.54, 128.19, 127.61, 125.57, 122.37, 61.01, 54.81, 53.44, 51.80, 38.39, 30.53, 22.38, 20.35 ppm. ESI-MS in MeOH (positive): *m/z* 291.6 ($[M + H]^+$). ESI-MS in MeOH (negative): *m/z* 289.3 ($[M – H]^–$).

$H_2L^1 \cdot 2.5H_2O$. To a solution of 2-hydroxy-3-methyl-(*S*)-pyrrolidine-2-carboxylate-5-methylbenzaldehyde (1.7 g, 6.5 mmol) in ethanol (30 mL) under stirring a solution of 4-*N*-pyrrolidine-3-thiosemicarbazide (0.94 g, 6.5 mmol) in ethanol (10 mL) was added. The reaction mixture was refluxed at 85 °C for 1 h. Upon cooling to the room temperature the precipitate was filtered off, washed with cold ethanol (5 mL) and dried in vacuo overnight. Yield: 0.7 g, 25.2%. Anal. Calcd for $C_{19}H_{26}N_4O_3S \cdot 2.5H_2O$ (*M* 435.54 g mol^{-1}), %: C, 52.40; H, 7.17; N, 12.86; S, 7.36. Found, %: C, 52.29; H, 7.20; N, 12.70; S, 7.19. IR (ATR, selected bands, ν_{max}): 3165, 3066, 2961, 2873, 1639, 1617, 1558, 1436, 1306, 1190, 961, 913, 757, 619, 575 cm^{-1}. UV–vis in MeOH, λ, nm (ε, M^{-1} cm^{-1}): 390 (1220), 334 (11350), 300sh (14000), 288 (16265), 249sh (10910), 227 (19380).^{1}H NMR (500.10 MHz, DMSO-*d*$_6$): δ 11.24 (s, 1H, NH), 8.47 (s, 1H, HC=N), 7.22 (s, 1H, Ar), 7.19 (s, 1H, Ar), 4.17 (d, *J* = 13.54 Hz, 1H, CH_2), 3.99 (d, *J* = 13.54 Hz, 1H, CH_2), 3.66 (s, 4H, proline or pyrrolidine), 3.56–3.52 (m, 2H, proline), 3.30–3.23 (m, 2H, proline), 2.85–2.77 (m, 1H, proline), 2.26 (s, 3H, CH_3), 2.21–2.12 (m, 1H, proline), 2.01–1.90 (m, 4H, pyrrolidine), 1.90–1.82 (m, 1H, proline), 1.75–1.65 (m, 1H, proline) ppm. ESI–MS in MeOH (positive): *m/z* 391 ($[H_2L^1 + H]^+$). Single

crystals of X-ray diffraction quality were obtained by slow diffusion of diethyl ether into ethanolic solution of H_2L^1.

$H_2L^2 \cdot 2H_2O$. To a solution of methyl[1-(3-formyl-2-hydroxy-5-methylbenzyl)-(*R*/*S*)-pyrrolidin-2-yl]acetate (0.40 g, 1.37 mmol) in ethanol (30 mL) was added 4-*N*-pyrrolidine-3-thiosemicarbazide (0.20 g, 1.37 mmol) in water (30 mL). The solution was stirred at 80 °C for 24 h and cooled to room temperature. The beige precipitate was filtered off, washed with diethyl ether (2 mL) and dried in vacuo. Yield: 0.24 g, 43%.; no m.p., decomposition without melting, onset at 170 °C. Anal. Calcd for $C_{20}H_{28}N_4O_3S \cdot 2H_2O$ (*M* 440.56 g mol^{-1}), %: C, 54.52; H, 7.32; N, 12.72; S, 7.28. Found, %: C, 54.36; H, 7.01; N, 12.33; S, 7.11. ^{1}H NMR (500.10 MHz, DMSO-d_6): δ 11.16 (br, 1H, N^2H), 8.47 (s, 1H, $C^{15}H$), 7.12 (s, 1H, C^4H + C^6H), 3.97 (d, *J* = 13.7 Hz, 1H, C^8H_2), 3.58-3.72 (br, 4H, $C^{17}H_2$ + $C^{20}H_2$), 3.60 (d, *J* = 13.6 Hz, 1H, C^8H_2), 3.04-2.97 (m, 1H, C^9H), 2.96-2.89 (m, 1H, $C^{12}H_2$), 2.44-2.33 (m, 3H, $C^{12}H_2$ + $C^{13}H_2$), 2.26 (s, 3H, C^7H_3), 2.10-2.00 (m, 1H, $C^{11}H_2$), 1.98-1.87 (br, 4H, $C^{18}H_2$ + $C^{19}H_2$), 1.76-1.63 (m, 2H, $C^{10}H_2$), 1.54-1.44 (m, 1H, $C^{11}H_2$) ppm. ^{13}C{1H} NMR (125.76 MHz, DMSO-d_6): δ 176.36, 173.45, 153.78, 146.35, 132.52, 129.54, 127.62, 124.91, 118.51, 61.17, 53.24, 51.38, 37.75, 30.63, 22.44, 20.51 ppm. ESI-MS in MeOH (positive): *m/z* 405.38 ($[M+H]^+$). Calcd for $C_{20}H_{29}N_4O_3S$: *m/z* 405.20. ESI-MS in MeOH (negative): *m/z* 403.19 ($[M–H]^–$). Calcd for $C_{20}H_{27}N_4O_3S$: *m/z* 403.18. IR (ATR, selected bands, ν_{max}): 3364, 2965, 2881, 1550, 1462, 1349, 1286, 915, 670, 607 cm^{-1}. UV–vis in MeOH, λ, nm (ε, M^{-1} cm^{-1}): 335 (14327), 300 (15771), 288 (20648), 227 (22884). For atom labeling scheme and assignment of NMR resonances see Chart 1.

Synthesis of Metal Complexes

$[Ni(H_2L^1)Cl]Cl \cdot 1.3H_2O$ (**1**·1.3H_2O). To a solution of $H_2L^1 \cdot 2H_2O$ (0.20 g, 0.47 mmol) in ethanol (20 mL) was added a solution of $NiCl_2 \cdot 6H_2O$ (0.12 g, 0.50 mmol) in ethanol (5 mL) and the reaction mixture was stirred at room temperature for 2 h. The solvent was removed on a rotary evaporator under reduced pressure. The residue was dissolved in methanol (2 mL) and the product precipitated by addition of diethyl ether (20 mL) was filtered off, washed with diethyl ether (5 mL) and dried in air. Yield 0.21 g, 82.2%; no m.p., decomposition without melting, onset at 260 °C. Anal. Calcd for $C_{19}H_{26}Cl_2NiN_4O_3S \cdot 1.3H_2O$ (*M* 543.52 g mol^{-1}), %: C, 41.99; H, 5.30; N, 10.31; S, 5.90; Cl, 13.05. Found, %: C, 41.82; H, 5.20; N, 10.49; S, 6.03; Cl, 13.30. IR (ATR, selected bands, ν_{max}): 3204, 3108, 1733, 1598, 1548,

1496, 1450, 1360, 1215, 1201, 1180, 915, 887, 862, 706, 603 cm^{-1}. UV–vis in MeOH, λ, nm (ε, M^{-1} cm^{-1}): 865 (135), 770 (87), 620 (45), 398 (33100), 293 (38900), 259 (62300), 236 (69600). ESI-MS in methanol (positive): *m/z* 447.26 $[Ni(HL^1)]^+$. Calcd for $C_{19}H_{25}NiN_4O_3S$ *m/z* 447.10. X-ray diffraction quality single crystals were grown by slow diffusion of diethyl ether into the solution of the complex in methanol. Magnetic susceptibility measurements indicate its diamagnetism in the solid state.

$[Pd(H_2L^1)Cl]Cl·H_2O$ (**2**·H_2O). To a solution of $H_2L^1·2H_2O$ (0.20 g, 0.47 mmol) in ethanol (20 mL) was added a solution of $PdCl_2$ (0.09 g, 0.51 mmol) in ethanol (5 mL) and the reaction mixture was refluxed for 1 h. The solvent was removed on a rotary evaporator under reduced pressure. The residue was dissolved in methanol (2 mL) and the product precipitated by addition of diethyl ether (20 mL) was filtered off, washed with diethyl ether (5 mL) and dried in air. Yield 0.13 g, 47.2%. Anal. Calcd for $C_{19}H_{26}Cl_2PdN_4O_3S·H_2O$ (*M* 585.84 g mol^{-1}), %: C, 38.95; H, 4.82; N, 9.56; S, 5.47; Cl, 12.10. Found, %: C, 39.15; H, 4.43; N, 9.56; S, 5.70; Cl, 12.40. IR (ATR, selected bands, ν_{max}): 3200, 3101, 1733, 1544, 1495, 1449, 1364, 1218, 1201, 1182, 1166, 863, 822, 600 cm^{-1}. UV–vis in MeOH, λ, nm (ε, M^{-1} cm^{-1}): 412 (22340), 320 (31575), 244 (60220). ^{1}H NMR (500.10 MHz, DMSO-d_6): δ 9.99 (br, 1H, N^2H), 8.31 (s, 1H, $C^{14}H$), 7.27 (d, *J* = 2.0 Hz, 1H, C^6H), 7.22 (d, *J* = 2.0 Hz, 1H, C^4H), 4.55–4.47 (m, 1H C^9H), 4.42 (1H dd, *J* = 13.0, 5.0 Hz, C^8Hb), 4.31 (C^8Ha dd, *J* = 13.0, 5.0 Hz, 1H), 3.64–3.55 (m, $C^{12}Hb$ 1H), 3.53–3.47 (m, $C^{16}H$ 2H), 3.43–3.34 (m, $C^{12}Ha$ 1H), 2.50–2.41 (m, $C^{10}H_b$ 1H), 2.21 (s, C^7H_3, 3H,), 2.11–1.98 (m, $C^{10}Ha$+$C^{11}Hb$, 2H), 1.94–1.86 (m, $C^{11}Ha$, 1H) ppm. ^{13}C NMR (126 MHz,) δ 171.20, 170.35, 158.62, 146.79, 137.09, 135.24, 122.92, 120.03, 118.87, 66.01 (C^9H), 62.69, 55.95(C^8H), 55.14($C^{12}H$), 51.24($C^{16}H$), 34.63, 28.42($C^{10}H$), 26.03($C^{17}H$), 22.86($C^{11}H$), 20.14(C^7), 14.29 ppm. ESI-MS in methanol (negative): *m/z* 530.93 $[M–HCl–H]^-$. Calcd for $C_{19}H_{24}N_4O_3PdS$ *m/z* 531.03. Single crystals were grown from dimethyl sulfoxide at room temperature.

$[Cu(H_2L^1)Cl]Cl·0.7H_2O$ (**3**·$0.7H_2O$). To a solution of $H_2L^1·2H_2O$ (0.20 g, 0.47 mmol) in ethanol (20 mL) was added a solution of $CuCl_2·2H_2O$ (0.09 g, 0.53 mmol) in ethanol (5 mL) and the reaction mixture was stirred at room temperature for 2 h. The solvent was removed on a rotary evaporator under reduced pressure. The residue was dissolved in methanol (2 mL) and the product precipitated by addition of diethyl ether (20 mL) was filtered off, washed with diethyl ether (5 mL) and dried in air. Yield 0.15 g, 59.4%. Anal. Calcd for $C_{19}H_{26}Cl_2CuN_4O_3S·0.7H_2O$ (*M* 537.56 g mol^{-1}), %: C, 42.45; H, 5.14; N, 10.42; S, 5.97; Cl,

13.19. Found, %: C, 42.30; H, 4.97; N, 10.24; S, 6.25; Cl, 13.54. IR (ATR, selected bands, ν_{max}): 3178, 3083, 1742, 1582, 1481, 1462, 1445, 1394, 1361, 1347, 1259, 1179, 911, 821, 759, 700, 576 cm^{-1}. UV–vis in MeOH, λ, nm (ε, M^{-1} cm^{-1}): 635 (279), 403 (13347), 333sh (10050), 311sh (21397), 299 (29236), 267 (18430), 260sh (18410). ESI-MS in methanol (positive): *m/z* 452 $[Cu(HL^1)]^+$.

$[Cu(H_2L^2)Cl]Cl·H_2O$ (**4**·H_2O). To a solution of H_2L^2 (95 mg, 0.24 mmol) in methanol (10 mL) was added $CuCl_2·2H_2O$ (44 mg, 0.26 mmol) in methanol (1 mL) and the reaction mixture was refluxed for 1 h. The green solution was concentrated to a volume of ca. 4 mL and allowed to stand at +4 °C for 6 h. The precipitate formed was filtered off, washed with diethyl ether (3 mL) and dried in vacuo. Yield: 70 mg, 55%; no m.p., decomposition without melting, onset at 220 °C. Anal. Calcd for $C_{20}H_{28}Cl_2CuN_4O_3S·H_2O$ (*M* 556.99 g mol^{-1}), %: C, 43.13; H, 5.43; N, 10.06; S, 5.76. Found, %: C, 43.03; H, 5.12; N, 9.68; S, 5.55. ESI-MS in MeOH (positive): *m/z* 466.31 ($[Cu(HL^2)]^+$). Calcd for $C_{20}H_{27}CuN_4O_3S$: *m/z* 466.11. ESI-MS in MeOH (negative): *m/z* 464.10 ($[Cu(L^2–H\ )]^-$), 500.05 ($[Cu(L^2)Cl]^-$). Calcd for $C_{20}H_{25}CuN_4O_3S$: *m/z* 464.09. Calcd for $C_{20}H_{26}ClCuN_4O_3S$: *m/z* 500.07. IR (ATR, selected bands, ν_{max}): 3397, 2875, 2608, 1741, 1582, 1483, 1346, 1175, 910, 820, 759 cm^{-1}. UV–vis in MeOH, λ, nm (ε, M^{-1} cm^{-1}): 616 (191) 403 (15457), 327 (14377), 297 (35476), 263 (24855). Solvent-free sample is stable up to 210 °C.

Crystallographic Structure Determination. X-ray diffraction measurements of H_2L^1 and **1** were performed on a Bruker D8 Venture, while those of **2** and **4** on Bruker X8 APEXII CCD and STOE diffractometers, all equipped with an Oxford Cryosystem cooler device. The single crystals of H_2L^1, **1**, **2** and **4** were positioned at 35, 35, 40 and 40 mm from the detector, and 1401, 1071, 636 and 2136 frames were measured, each for 20, 10, 20 and 38 s over 0.4, 0.5, 1 and 1° scan width, respectively. The data were processed using SAINT software.[25] Crystal data, data collection parameters, and structure refinement details are given in Table 1. The structures were solved by direct methods and refined by full-matrix least-squares techniques. All non-hydrogen atoms were refined with anisotropic displacement parameters. H atoms were inserted in calculated positions and refined with a riding model. The pyrrolidine and proline rings in one one of the two crystallographically independent molecules of **1** were found to be disordered over two positions with s.o.f. 0.65:0.35 and 0.75:0.25, respectively, without using any restraints implemented in *SHELXL*2014. SADI and EADP restraints were applied to resolve the static disorder observed in the co-crystallized

solvent molecules in H_2L^1. The single crystal of **4** was weakly diffracting and the resolution of the collected X-ray data was estimated to be 1.02 Å. Nevertheless, the structure could be solved and electron density of the molecule is well-defined, allowing for the determination of the atomic connectivity and refinement with anisotropic temperature factors for all non-hydrogen atoms. The following software programs and computer were used: structure solution, *SHELXS-97*; refinement, *SHELXL-97*;[26] molecular diagrams, *ORTEP-3*;[27] computer, Intel CoreDuo. CCDC1471829–1471831 and 1492553.

.

Table 1. Crystal data and details of data collection for H_2L^1, **1**, **2** and **4**.

Compound	H_2L^1	**1**	**2**	**4**
empirical formula	$C_{20.25}H_{31}N_4O_{4.25}S$	$C_{19}H_{26}Cl_2N_4O_3NiS$	$C_{19}H_{26}Cl_2N_4O_3PdS$	$C_{20}H_{28}Cl_2CuN_4O_3S$
Fw	430.55	520.11	567.80	538.96
space group	*C*2	$P2_1$	$P2_1$	*C*2/*c*
a [Å]	10.5018(4)	6.9292(2)	6.9628(5)	20.3880(16)
b [Å]	24.7063(9)	18.4742(8)	18.5602(13)	14.1122(7)
c [Å]	16.9193(7)	17.4103(7)	17.4498(12)	15.9901(12)
β [°]	90.967(2)	101.171(2)	101.011(2)	100.503(6)
V [Å^3]	4389.3(3)	2186.49(14)	2213.5(3)	4523.6(5)
Z	8	4	4	8
λ [Å]	0.71073	0.71073	0.71073	1.54186
ρ_{calcd} [g cm^{-3}]	1.303	1.580	1.704	1.583
crystal size [mm]	0.20 × 0.13 × 0.12	0.32 × 0.20 × 0.20	0.15 × 0.05 × 0.05	0.08 × 0.04 × 0.02
T [K]	100(2)	130(2)	100(2)	100(2)
μ [mm^{-1}]	0.182	1.257	1.203	4.658
R_1[a]	0.0543	0.0341	0.0418	0.0555
wR_2[b]	0.1493	0.0826	0.0899	0.1307
Flack parameter	0.01(7)	−0.02(3)	−0.04(2)	
GOF[c]	1.029	1.023	1.023	0.942

[a] $R_1 = \Sigma||F_o| - |F_c||/\Sigma|F_o|$. [b] $wR_2 = \{\Sigma[w(F_o^2 - F_c^2)^2]/\Sigma[w(F_o^2)^2]\}^{1/2}$. [c] GOF = $\{\Sigma[w(F_o^2 - F_c^2)^2]/(n - p)\}^{1/2}$, where *n* is the number of reflections and *p* is the total number of parameters refined.

One-dimensional ^{1}H and ^{13}C NMR and two-dimensional $^{1}H–^{1}H$ COSY and $^{1}H–^{13}C$ HMBC NMR spectra were recorded on two Bruker Avance III spectrometers at 500.32 or 500.10 (^{1}H) and 125.82 or 125.76 (^{13}C) MHz, respectively, at room temperature, and using standard pulse programs. ^{1}H and ^{13}C shifts are quoted relative to the solvent residual signals. Electrospray ionization mass spectrometry (ESI-MS) was carried out with a Bruker Esquire 3000 instrument and the samples were dissolved in methanol. Elemental analyses were performed at the Microanalytical Laboratory of the University of Vienna with a Perkin Elmer 2400 CHN Elemental Analyzer (Perkin Elmer, Waltham, MA). IR spectra were measured on a Bruker Vertex 70 Fourier transform IR spectrometer by using the ATR technique. UV–vis absorption spectra were recorded on JASCO V770 spectrophotometer, while CD spectra on JASCO J1500 spectrometer. The spectra were measured at room temperature in a cuvette with 10 mm path length.

Antiproliferative activity. CH1 cells (human ovarian carcinoma) were a generous gift from Lloyd R. Kelland, CRC Centre for Cancer Therapeutics, Institute of Cancer Research, Sutton, UK. SW480 (human adenocarcinoma of the colon) and A549 (human nonsmall cell lung cancer) cells were kindly provided by Brigitte Marian (Institute of Cancer Research, Department of Medicine I, Medical University of Vienna, Austria). NIH/3T3 (ATCC CRL-1658) mouse embryonic fibroblasts were cultured according to the ATCC (American Type Culture Collection) protocol. All cell culture media and reagents were purchased from Sigma-Aldrich Austria and plastic ware from Starlab Germany. CH1, SW480, A549 cells were grown in 75 cm² culture flasks as adherent monolayer cultures in Minimum Essential Medium (MEM) supplemented with 10% heat-inactivated fetal calf serum, 1 mM sodium pyruvate, 4 mM L-glutamine and 1% non-essential amino acids (from 100x ready-to-use stock). NIH/3T3 cells were maintained in Dulbecco's Modified Eagle's Medium (DMEM) supplemented with 10% of bovine calf serum. Cultures were maintained at 37 °C in humidified atmosphere containing 95% air and 5% CO_2.

Cytotoxic effects of the test compounds were determined by means of a colorimetric microculture assay [MTT assay; MTT = 3-(4,5-dimethyl-2-thiazolyl)-2,5-diphenyl-2H-tetrazolium bromide]. Cisplatin (Teva) was used as a positive control. Cells were harvested from culture flasks by trypsinization and seeded by using a pipetting system (Biotek Precision XS Microplate Sample Processor) in densities of 3×10^3 (A549), 1×10^3 (CH1) and 2×10^3 (SW480) in 100 µL/well aliquots in 96-well microculture plates. For 24 h, cells

were allowed to settle and resume proliferation. Test compounds were then dissolved in DMSO, diluted in complete culture medium and added to the plates where the final DMSO content did not exceed 0.5%. After 96 h of drug exposure, the medium was replaced with 100 μL/well of a 1:7 MTT/RPMI 1640 mixture (MTT solution, 5 mg/mL of MTT reagent in phosphate-buffered saline; RPMI 1640 medium, supplemented with 10% heat-inactivated fetal bovine serum and 4 mM L-glutamine), and plates were incubated for further 4 h at 37 °C. Subsequently, the solution was removed from all wells, and the formazan crystals formed by viable cells were dissolved in 150 μL of DMSO per well. Optical densities at 550 nm were measured with a microplate reader (Biotek ELx808) by using a reference wavelength of 690 nm to correct for unspecific absorption. The quantity of viable cells was expressed relative to untreated controls, and 50% inhibitory concentrations (IC_{50}) were calculated from concentration-effect curves by interpolation. Evaluation is based on means from three independent experiments. A slightly modified procedure was used to test the antiproliferative effect in NIH/3T3 mouse embryonal fibroblast cells, which is provided in the SI.

Mechanisms of cell death: assay for apoptosis induction. The assay was carried out using Annexin V-FITC Apoptosis Detection Kit Cat. No. PF 032 from Calbiochem according to the manufacturer's instructions. The concentration of the A549 cell suspension was adjusted to approximately 0.5×10^6 cells/mL in MEM and the cell suspension was distributed into 1 mL aliquots to a 24-well plate, then incubated overnight at 37 °C, 5% CO_2. On the following day, the medium was removed and replaced by 1 mL MEM containing the compounds except the control samples. A549 cells were incubated in the presence of the compounds at 20 μM in the 24-well plate for 3 h at 37°C, 12H-benzo[α]phenothiazine (M627)[28] and cisplatin (Teva) at 20 μM were used as positive controls. After the incubation period the samples were washed with PBS and fresh MEM medium was added to the samples. The cells were incubated overnight at 37 °C, 5% CO_2. On the following day, 200 μL 0.25% Trypsin (Trypsin-Versen) was added to the samples until cells appeared detached followed by the addition of 400 μL of MEM supplemented with 10% bovine serum. The cells were collected to Eppendorf tubes and centrifuged at 2000 g for 2 min. The harvested cells were resuspended in fresh serum free MEM culture medium. After this step, the apoptosis assay was carried out according to the rapid protocol of the kit. The fluorescence was analyzed immediately using a ParTec CyFlow flow cytometer (Partec GmbH, Münster, Germany).

Results and Discussion

Synthesis and Characterization of Ligands and Metal Complexes. The chiral 2-hydroxy-3-methyl-(*S*)-pyrrolidine-2-carboxylate-5-methylbenzaldehyde 4-*N*-pyrrolidine-3-thiosemicarbazone has been prepared in three steps as described recently for unsubstituted at terminal nitrogen atom of the thiosemicarbazide moiety derivative.[19] First 3-chloromethyl-2-hydroxy-5-methylbenzaldehyde[22] was allowed to react with L-proline methyl ester hydrochloride in the presence of triethylamine with formation of the desired conjugate. Condensation reaction of this latter compound with 4-*N*-pyrrolidine-3-thiosemicarbazide[20] followed by hydrolysis of the methyl ester group afforded the corresponding TSC with coupled *via* a methylene group L-Pro moiety (H_2L^1). The formation of desired species has been confirmed by ^1H and ^{13}C NMR measurements, as well as by ESI mass spectra. The mass spectrum recorded in positive ion mode showed peaks at *m*/*z* 391 due to $[M+H]^+$ ion. Aqueous solution of H_2L^1 at neutral pH is optically active. The second optically active ligand H_2L^2 was obtained similarly by using the (*R*/*S*)-β^3-homoproline methyl ester instead of the L-proline methyl ester hydrochloride. The latter was prepared *via* a four-step procedure by exploring the Arndt-Eistert reaction as a common method of homologization of an α-amino acid into β-amino acid (*e.g.*, proline to β^3-homoproline) as shown in Scheme S1.[24] Briefly, in the first step the secondary amine in L-proline was protected by reaction with benzyl chloroformate in aqueous KOH solution. Then the *N*-protected L-proline was converted into the acyl halide by treating with excess oxalylchloride in dichloromethane followed by methylation with TMS-diazomethane and formation of the α-diazotylketone. This latter conversion called Wolff rearrangement is the key step involving the insertion of CH_2-group.[29] The α-diazotylketone was further rearranged in dry methanol in the presence of silver benzoate and triethylamine. Finally the amino group was deprotected with H_2 in the presence of 10% PdC in dry methanol. The synthesis can be performed in large scale with 51% overall yield of β^3-homoproline methyl ester. The reaction of β^3-homoproline methyl ester with 3-chloromethyl-2-hydroxy-5-methylbenzaldehyde in THF/CH_2Cl_2 afforded [1-(3-formyl-2-hydroxy-5-methylbenzyl)-(*R*/*S*)-pyrrolidin-2-yl]acetic acid methyl ester purified by column chromatography giving an orange oil in 80% yield. Condensation of this product with 4-*N*-pyrrolidine-3-thiosemicarbazide accompanied by hydrolysis of the ester group resulted in H_2L^2 in 43% yield. The formation of the desired ligand precursor was confirmed by ESI mass spectrometry which showed the presence of a peak with *m/z* 405, attributed to $[M+H]^+$ ion, as well as by ^1H and ^{13}C NMR spectra.

By reaction of H_2L^1 with $NiCl_2{\cdot}6H_2O$ in ethanol at room temperature the red complex $[Ni(H_2L^1)Cl]Cl{\cdot}1.3H_2O$ was synthesized in 82% yield. Similarly starting from $PdCl_2$ and $CuCl_2{\cdot}2H_2O$ the complexes $[Pd(H_2L^1)Cl]Cl{\cdot}H_2O$ and $[Cu(H_2L^1)Cl]Cl{\cdot}0.7H_2O$ were isolated in 47 and 59% yield, respectively. ESI mass spectra of **1** and **3** measured in the positive ion mode exhibit a strong peak at *m/z* 447.26 and *m/z* 452, which can be assigned to $[Ni(HL^1)]^+$ and $[Pd(HL^1)]^+$, respectively, while the negative ion mass spectrum of **2** contains a strong signal at *m/z* 530.93 due to $[Pd(L^1)Cl]^-$. By reaction of a methanolic solution of $CuCl_2{\cdot}2H_2O$ with H_2L^2 the complex $[Cu(H_2L^2)Cl]Cl{\cdot}H_2O$ was obtained in 55% yield. ESI mass spectrum, recorded in positive ion mode, showed the presence of a strong peak at *m*/*z* 466.31 attributed to $[Cu^{II}(HL^2)]^+$, while in negative ion mode peaks with *m*/*z* 464.10 and 500.05 due to $[Cu^{II}(L^2{-}H)]^-$ and $[Cu^{II}(L^2)Cl]^-$ respectively, were observed in agreement with the proposed structure.

X-ray crystallography. Figure 1 shows the structure of the chiral ligand precursor H_2L^1 with selected bond distances and angles quoted in the legend. The compound crystallizes in the monoclinic space group *C*2 with two crystallographically independent molecules in the asymmetric unit. The conformation adopted by H_2L^1 is very close to that of the ligand in complexes **1** and **2** (vide infra). The prolinic moiety is in the zwitterionic form, what makes atom N4a in addition to C14a chiral. A strong intramolecular hydrogen bonding O1a–H···N1a with O1a···N1a 2.595(4) Å and O1a–H···N1a 143.4° is evident in the structure of H_2L^1. The atoms N2a and N4a act as proton donors to $O3a^i$(–*x* + 1, *y*, –*z* + 1) and $O2b^i$(–*x* + 1, *y*, –*z* + 1), respectively, forming hydrogen bonds N2a–H···$O3a^i$ and N4a–H···$O2b^i$ with N2a···$O3a^i$ 2.736(5) Å, N2a–H···$O3a^i$ 155.5° and N4a···$O2b^i$ 2.857(5) Å, N2a–H···$O3a^i$ 136.7°.

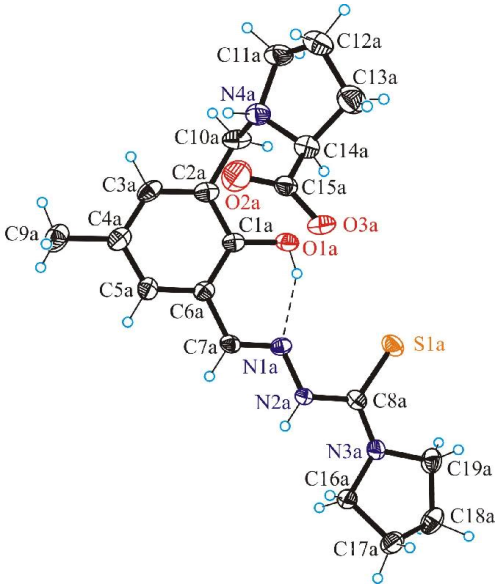

Figure 1. ORTEP view of H_2L^1 with thermal displacement parameters drawn at the 50% probability level. Selected bond distances (Å) and torsion angles (deg): C1a–O1a 1.352(4), N1a–N2a 1.367(3), N2a–C8a 1.368(4), C8a–S1a 1.694(3), C8a–N3a 1.335(4); $\Theta_{C1a–C2a–C10a–N4a}$ –91.6(3); $\Theta_{C10a–N4a–C14a–C15a}$ –100.8(3).

The results of X-ray diffraction studies of **1**, **2** and **4** are shown in Figures 2 and 3. The compounds **1** and **2** are isostructural and crystallized in the noncentrosymmetric monoclinic space group $P2_1$ as pure enantiomers, as also confirmed by the Flack parameters quoted in Table 1, with two chiral atoms of the same configuration (vide infra). Complex **4** crystallized in the centrosymmetric monoclinic space group $C2/c$. The asymmetric unit in **1** and **2** consists of two crystallographcally independent cations $[M(H_2L^1)Cl]^+$ (M = Ni, Pd) and two chloride counterions, where H_2L^1 is the charge-neutral proline-thiosemicarbazone hybrid, while that of **4** of one complex $[Cu(H_2L^2)Cl_2]$. The ligands H_2L^1 in **1** and **2** and, H_2L^2 in **4** act as tridentate binding to the metal(II) *via* phenolate oxygen atom O1, nitrogen atom N1 and thione sulfur S1 as shown in Figures 2 and 3 for one of the two crystallographically independent cations $[Ni(H_2L^1)Cl]^+$, $[Pd(H_2L^1)Cl]^+$ and complex $[Cu(H_2L^2)Cl_2]$. The ligands are deprotonated at O1, but protonated at N4, so that the overall protonation level does not change. Protonation at N4 makes this atom chiral (*S* configuration) in **1** and **2**. The second chiral centre C14 has the same *S* configuration. According to the literature the nitrogen atom of L-prolinate ligand or moiety upon coordination to metal ion or protonation in most cases adopts the same configuration as the asymmetric carbon atom,[30] although cases when the two atoms adopt opposite configurations are also known.[31] The coordination geometry of nickel(II) and palladium(II) is square-planar. The fourth coordination place is occupied by a chlorido ligand.

The overall positive charge of the complex cation is counterbalanced by another chloride ion. The Pd−O, Pd−N, Pd−Cl and Pd−S bond lengths in **2** are well-comparable to those found in complex [Pd(HSal4Et)Cl]·H_2O, where H_2Sal4Et = 2-hydroxybenzaldehyde 4-*N*-ethylthiosemicarbazone, at 2.019(2), 1.965(2), 2.3078(8) and 2.2456(9) Å, respectively.[32] The protonated atom N4a in cation A acts as proton donor in bifurcated hydrogen bonding interaction to O2a and $Cl2^{i}$ ($x - 1$, y, $z - 1$), while N4b in cation B to O1B and O2B as shown in Figure S1. In addition, strong hydrogen bonding interactions N2a−H···Cl2a [N2a···Cl2a 3.157(6) Å, N2a−H···Cl2a 160.2°], N2b−H···$Cl2b^{ii}$ ($-x + 1$, $y - 0.5$, $-z + 1$) [N2b···$Cl2b^{ii}$ 3.162(0) Å, N2b−H···$Cl2b^{ii}$ 156.5°] and O3b−H···$Cl2a^{ii}$ ($-x + 1$, $y + 0.5$, $-z + 1$) [O3b···$Cl2a^{ii}$ 2.926(0) Å, O3b−H···$Cl2a^{ii}$ 170.4°] are evident in the crystal structure of **2**. Closely similar hydrogen bonding interactions for **1** are quoted in Table S1.

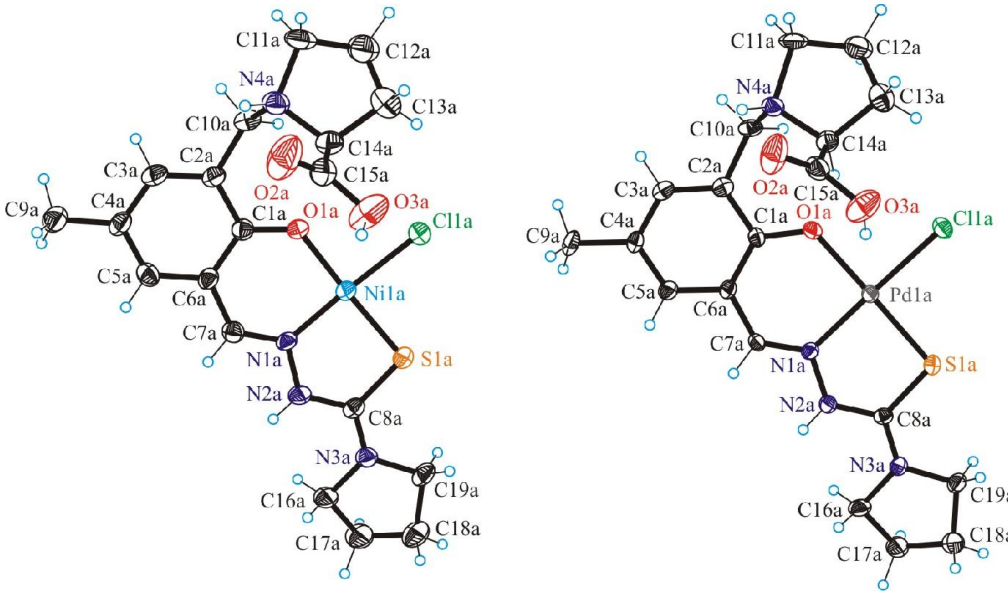

Figure 2. ORTEP view of one of the two crystallographically independent complex cations in the asymmetric unit of [Ni(H_2L^1)Cl]Cl (left) and [Pd(H_2L^1)Cl]Cl (right) with atom labeling schemes; thermal ellipsoids were drawn at 50% probability level. Selected bond distances (Å) and bond angles (deg) [Ni(H_2L^1)Cl]Cl: Ni1a−Cl1a 2.184(3), Ni1a−O1a 1.858(7), Ni1a−N1a 1.848(10), Ni1a−S1a 2.147(3), C1a−O1a 1.300(14), N1a−N2a 1.392(12), N2a−C8a 1.340(15), C8a−S1a 1.708(13), C8a−N3a 1.311(15); O1a−Ni1a−N1a 93.6(4), N1a−Ni1a−S1a 88.8(3). Selected bond distances (Å) and bond angles (deg) [Pd(H_2L^1)Cl]Cl: Pd1a−Cl1a 2.3049(12), Pd1a−O1a 2.016(3), Pd1a−N1a 1.976(4), Pd1a−S1a 2.2470(11), C1a−O1a 1.320(5), N1a−N2a 1.382(5), N2a−C8a 1.350(5), C8a−S1a 1.722(5), C8a−N3a 1.318(5); O1a−Pd1a−N1a 92.39(14), N1a−Pd1a−S1a 86.53(11).

A feature of note is the presence of short intermolecular contacts Ni···S and Pd···S between neighbouring complex cations of *ca.* 3.69 – 3.70 and 3.59 – 3.60 Å, respectively, as shown in Figures S2 and S3. The interplanar separation between aromatic ring of the interacting species is *ca.* 3.25 and 3.16 Å, in **1** and **2**, respectively. Formation of short contacts of this type is not characteristic for the complex [Pd(HSal4Et)Cl]·H_2O mentioned previously.

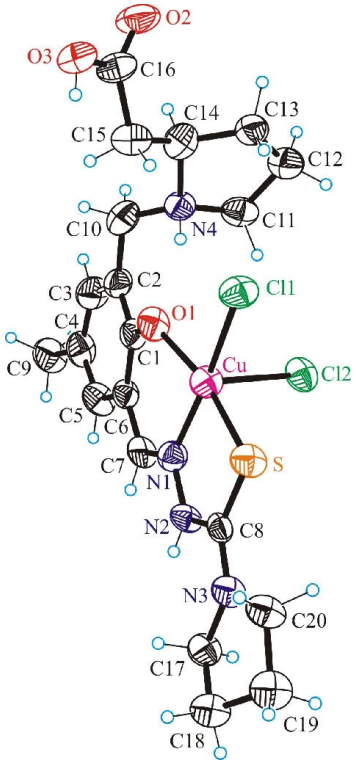

Figure 3. ORTEP view of **4** with atom labeling schemes; thermal ellipsoids were drawn at 50% probability level. Selected bond distances (Å) and bond angles (deg): Cu−Cl1 2.294(2), Cu−Cl2 2.732(3), Cu−N1 2.001(8), Cu–O1 1.916(6), Cu−S 2.262(3), C1−O1 1.339(11), N1−N2 1.373(10), N2−C8 1.376(11), C8−S 1.702(10), C8−N3 1.320(12); O1−Cu−N1 90.3(3), N1−Cu−S 86.1(2).

The coordination polyhedron of copper(II) in **4** is best described as a square-pyramid (τ = 0.15).[33] The tridentate ligand H_2L^2 and one chloride occupy the basal plane, while second chlorido ligand the apical position. Comparison of the bond lengths Cu–Cl1 and Cu–Cl2 (see legend to Figure 3) indicates markedly weaker binding of the apical chlorido ligand to copper(II). The protonated atom N4 acts as proton donor in intramolecular bifurcated hydrogen bonding interaction to O1 and Cl2 [N4···O1 2.624(10) Å, N4–H···O1 132.5°; N4···Cl1 3.684(8) Å, N4–H···Cl1 149.0°]. In addition, strong intermolecular hydrogen bonding interactions N2−H···$Cl2^{ii}$ (−*x* + 1, −*y* + 1, −*z*) [N2···$Cl2^{ii}$ 3.197(8) Å, N2−H···$Cl2^{ii}$

156.6°] and O3−H···Cl2^{i} (x, $-y$ + 1, z + 0.5) [O3···Cl2^{i} 2.925(7) Å, O3−H···Cl2^{i} 167.5°] are evident in the crystal structure of **4**.

NMR spectroscopy. The ^{1}H NMR spectra of **2** and H_2L^1 have been analyzed. The 2D homonuclear COSY ^{1}H–^{1}H and heteronuclear HMBC ^{1}H–^{13}C correlations were applied to assign the NMR signals (see Figure S4). The NMR spectra of H_2L^1 are consistent with X-ray diffraction structure. We note here the particular splitting of protons of the methylene group which connects the aromatic and proline rings. The two protons C^{8}**H**$_a$ and C^{8}**H**$_b$ are magnetically inequivalent due to their different spatial orientation with respect to the bond C^{8}H$_2$–N^{4}C^{9}C^{12}. The simulation of the ^{1}H NMR spectra (Figure 4) resulted in the geminal $^{2}J_{C8Ha\text{-}C8Hb}$ constant of 13 Hz and chemical shifts δ_{C8Ha} = 4.177 and δ_{C8Hb} = 4.005 ppm. The proton in α position (C^{9}**H** δ_{C9H} = 3.554 ppm) of the proline ring is split due to its vicinal proton-proton interaction with the two protons C^{10}**H**$_2$. The approximate dihedral angle for the adopted in this case conformation (Figure 4, right part) can be calculated by using the Karplus equation:[34,35]

$$ {}^{3}J = \begin{cases} 8.5 * cos^2\varphi - 0.28 & 0° \leq \varphi \leq 90° \\ 9.5 * cos^2\varphi - 0.28 & 90° \leq \varphi \leq 180° \end{cases} $$

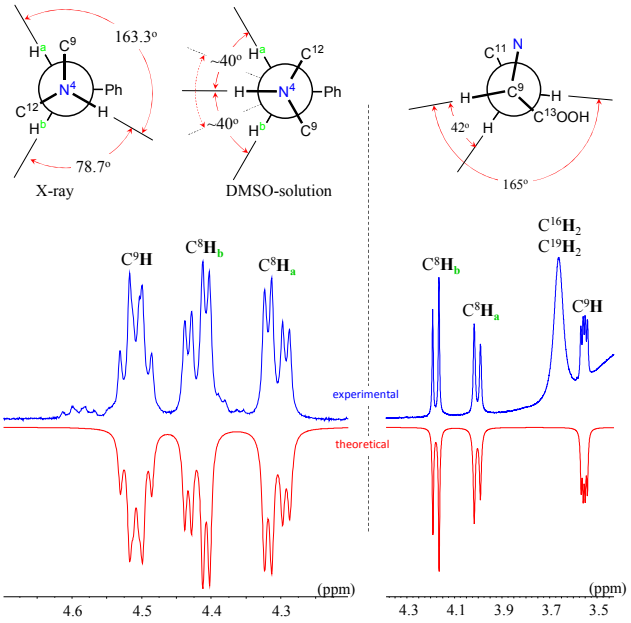

Figure 4. Experimental (500 MHz) and simulated ^{1}H NMR spectra of **2** (left) and H_2L^1 (right).

The conformation of the proline ring in H_2L^1 is consistent with previously reported data.[36,37] As can be seen from Figure 3, the C^8H_2 group in **2** has different splitting pattern and chemical shift in comparison with H_2L^1. A similar change in chemical shift is observed for $C^9\mathbf{H}$. The downfield shift of proton resonances of the proline ring in **2** can be related to double protonation of the proline group (amine nitrogen and carboxylato group) in the complex in comparison to single protonation in the zwitterionic form of the ligand. The single crystal X-ray analysis shows that the proline nitrogen (N^4) is protonated both in H_2L^1 and in **2.** In the case of complex **2** additional protonation of the ligand at O3a is also proved by X-ray analysis. The protonation state of N^4 is also preserved in solution (DMSO), in accord with the additional splitting of two protons of $C^8\mathbf{H}_2$ group. The modification in the splitting pattern of $C^8\mathbf{H}_2$ signals can be associated with the change of spatial orientation of $C^8\mathbf{H}_2$ group after coordination. According to the simulation of the NMR spectra the best fit between theoretical and experimental spectra indicates the same magnitude of vicinal coupling constant between the protons $C^8\mathbf{H}_a$ and $\mathbf{H}N^4$ and $C^8\mathbf{H}_b$ and $\mathbf{H}N^4$ and corresponds to the dihedral angle of 40° ($^3J_{C8\mathbf{H}\text{-}\mathbf{H}N4}$ = 5.0 Hz) (Figure 3). This value indicates an average position between free rotations around C^8H_2–$N^4C^9C^{12}$ single bond on the time scale of NMR spectroscopy. The protonation also affects the splitting of the α proton ($C^9\mathbf{H}$), and all ^{1}H NMR resonances are upfield shifted ($\delta_{C8\mathbf{H}a}$ = 4.419, $\delta_{C8\mathbf{H}b}$ = 4.307 and $\delta_{C9\mathbf{H}}$ = 4.509 ppm). The $\mathbf{H}N^4$ signal appears in the ^{1}H NMR spectra at 9.97 ppm as broad signal (13.0 Hz) as a consequence of splitting and chemical exchange in solution. The correlations between $\mathbf{H}N^4$ with $C^8\mathbf{H}_2$ and $C^9\mathbf{H}$ were confirmed by the presence of cross peaks in COSY ^{1}H–^{1}H spectra (Figure S5). The geminal $^2J_{\mathbf{H}a\text{-}\mathbf{H}b}$ constant is of the same magnitude of 13.0 Hz.

Dissolution of red solid of **1** in methanol resulted in formation of a green solution suggesting a change in coordination geometry of Ni(II). ^{1}H NMR spectrum of **1** showed broad lines, which indicated the presence of paramagnetic species in solution. We have determined the effective magnetic moment of **1** in CD_3OD (1.58×10^{-2} *M*) at 298 K by using the NMR method of Evans.[38] The value amounts to 3.26 B.M., which is typical for octahedral nickel(II) complexes with d^8 electronic configuration.[39] The CD spectrum of a methanolic solution of **1** (Figure 4, green trace) indicates the presence of asymmetric centers in the molecule. The CD signals are correlated to the absorption bands for the ligand precursor and show the absence of CD signals in the visible region. The absence of CD signals in the visible region of the

spectrum indicates that the proline moiety with its two asymmetric centers is not bound to the nickel(II) in solution.

The electronic absorption spectrum of **1** in methanol in the visible and NIR regions shows three bands with λ_{max} at 865 (11560 cm^{-1}), 770 (12987 cm^{-1}) and 620 (16129 cm^{-1}) nm (Figure 5) which can be attributed to $^3A_{2g} \rightarrow {}^3T_{2g}(F)$, $^3A_{2g} \rightarrow {}^1E_g(D)$ and $^3A_{2g} \rightarrow {}^3T_{1g}(F)$ transitions of Ni(II) in octahedral environment, respectively.[40] Spin-allowed transitions are known to give broad absorption bands, while spin-forbidden transitions are usually sharp.[41] For nickel(II) (d^8) in octahedral environment $^3A_{2g}$ is the ground term and the spin allowed transition $^3A_{2g} \rightarrow {}^3T_{2g}(F)$ is equal to the value of the crystal field splitting (10Dq).[42] The value (11560 cm^{-1}) is consistent with those reported for octahedral nickel(II) complexes.[43] The third characteristic transition $^3A_{2g} \rightarrow {}^3T_{1g}(P)$ is expected in the range of 19000 – 27000 cm^{-1}, which is obscured by strong intraligand absorption bands.

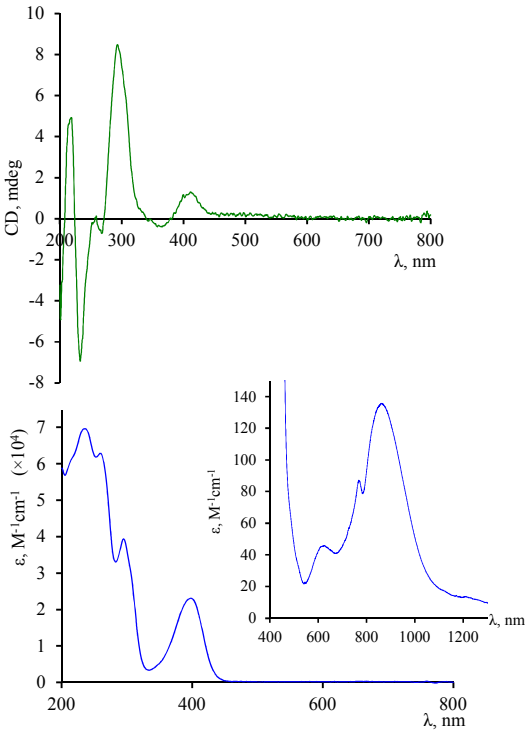

Figure 5. CD (green trace) and UV-vis absorption spectra (blue trace) of **1** in methanol.

Stability in aqueous solution. Quite recently we reported on complexation reactions of copper(II) with L-Pro-STSC in 30% (w/w) DMSO/H_2O.[19] Several determined thermodynamic cumulative stability constants (log β([CuLH]) = 21.58(3), log β([CuL]) =

17.54(3) and log β([CuLH$_{-1}$]) = 6.97(4)) along with the computed pM (= –log[M]) value of 13.4 (pH 7.4, c_{Cu} = 1 μM; c_L/c_{Cu} = 10) undoubtedly indicate significantly high stability of copper(II) complexes, which are closely related to those studied in this work (**3** and **4**). In addition, we monitored the behavior of **4** in aqueous solution with 1% DMSO by UV–vis spectroscopy. The data (Figure S7) indicates that the complex remains intact over 24 h in solution.

Cytotoxicity and mechanism of cell death. The antiproliferative activity of two organic hybrids H_2L^1 and H_2L^2 and four metal complexes **1**−**4** was investigated in the human cancer cell lines A549 (nonsmall cell lung carcinoma), CH1 (ovarian carcinoma) and SW480 (colon carcinoma) by means of the colorimetric MTT assay. Generally, CH1 cells are more sensitive to the compounds investigated in this work, giving up to 5 times lower IC_{50} values than SW480 cells, while A549 cells are less sensitive giving up to 9 times higher IC_{50} values than SW480 cells. The ligand precursors H_2L^1 and H_2L^2 and complexes **1**−**4** show different cytotoxic potencies, with IC_{50} values ranging from 0.9 to 308 μM (Table 2). The following structure-activity relationships are of note: (i) impact of metal coordination as compared to the uncomplexed ligand precursors; (ii) negligible role of square-planar coordination geometry of metal complexes in underlying mechanism of their cytotoxicity; (iii) the impact of substitution at terminal nitrogen atom of thiosemicarbazide moiety and (iv) the effect of increasing the structural flexibility of amino acid moiety by insertion of methylene group between the pyrrolidine ring and carboxylic group (proline *vs* homoproline). The impact of the central metal ion identity on the activity of ligands H_2L^1 and H_2L^2 are pronounced, and notably they are divergent for H_2L^1. Complexation of H_2L^1 to nickel(II) and palladium(II) weakens markedly the antiproliferative activity in all three cell lines, in line with other reported data.[44] The IC_{50} values of the nickel(II) complex **1** indicate roughly 10- (A549), 7.5- (CH1) and 2.7-fold (SW480) reduction and those of palladium(II) complex **2** a 13- (A549), 23- (CH1) and 26-fold (SW480) drop of cytotoxicity when compared to that of H_2L^1. In contrast, complexation of H_2L^1 to copper(II) results in a 9.5- (A549), 3- (CH1) and 10-fold (SW480) increase of cytotoxicity based on IC_{50} values. Similarly, complexation of H_2L^2 to copper(II) gives a 3.8- (A549), 3.4- (CH1) and 8.6-fold (SW480) increase of cytotoxicity. Since complexes **1**−**3** are square-planar based on X-ray diffraction data of **1** and **2**, and X-ray crystallography data on previously studied copper(II) complex [Cu(D-Pro-STSC)Cl]Cl,[19] which is closely related to **3** and **4**, we can conclude that the role of coordination geometry in

the underlying mechanism of cytotoxicity seems to be marginal, if any, if we compare the IC_{50} values of **1**−**3** with that of H_2L^1. This conclusion remains valid, if we exclude **1** from the series due to the change in coordination geometry in solution to octahedral. Substitution at the terminal nitrogen atom of thiosemicarbazide moiety, namely pyrrolidine *vs* NH_2 has a marked effect on cytotoxicity as well, which can be compared with that of metal coordination. A 23- (CH1) and more than 10-fold (SW480) decrease of IC_{50} values is achieved *via* this substitution for metal-free compounds, and a 5 to 5.5-fold decrease for the same structural modification in copper(II) complexes.[19] Insertion of a CH_2 group between the pyrrolidine ring and COOH group of amino acid moiety reduces markedly the antiproliferative activity of both ligand precursor and its copper(II) complex. Based on IC_{50} values a maximal 8-fold drop of cytotoxicity was observed on going from **3** to **4**. Antiproliferative activity of complex **3** is slightly lower, but comparable to the clinical drug cisplatin. Compounds found to be active (H_2L^1, H_2L^2, complexes **3** and **4**) in human cancer cells were tested for their antiproliferative activity in non-cancerous mouse embryonal fibroblast (NIH/3T3) cell lines as well. These compounds showed no selectivity as their activity in the normal cells is comparable to that obtained for the tumor cells.

Table 2. Inhibition of cancer cell growth of ligand precursors and metal complexes in human non-small cell lung (A549) carcinoma cell lines, ovarian (CH1), colon (SW480) and NIH/3T3 mouse embryonal fibroblast cells; 50% inhibitory concentrations (means ± standard deviations), obtained by the MTT assay (exposure time 96 h).

	IC_{50} value ± SD			
	A549	CH1	SW480	NIH/3T3[a]
H_2L^1	22.9 ± 3.0	2.7 ± 0.2	9.8 ± 1.0	21.0 ± 1.0
H_2L^2	72 ± 5	6.7 ± 0.1	32 ± 2	34.7 ± 0.2
1	226.2 ± 17.1	20.3 ± 4.5	26.0 ± 4.3	–
2	307.9 ± 6.5	62.0 ± 3.3	252.1 ± 19.6	–
3	2.4 ± 0.3	0.90 ± 0.08	0.99 ± 0.09	3.4 ± 0.3
4	19 ± 3	2.0 ± 0.1	3.7 ± 0.1	13.8 ± 0.8
$CuCl_2{\cdot}2H_2O$[b]	–	43 ± 3	> 160	–
cisplatin	1.3± 0.4[c]	0.16± 0.03[c]	3.5± 0.3[c]	2.3± 0.4

[a] Applied protocol described in the SI. [b] Taken from ref.[44]. [c] Taken from ref.[45]

The mechanism of cytotoxicity induced by complexes (H_2L^1, H_2L^2, complexes **3** and **4**) was assessed by analysis of A549 cells stained for Annexin-V and and propidium iodide (PI) using flow cytometry. Compounds M627 and cisplatin were used as positive controls. Apoptosis is a fundamental mode of cell death which performs a regulatory function during normal development, in tissue homeostasis, and in some disease processes. In normal viable cells phosphatidyl serine (PS) is located on the cytoplasmic surface of the cell membrane. Upon induction of apoptosis, rapid alterations in the organisation of phospholipids in most cell types occurs leading to exposure of PS on the cell surface. In this assay a fluorescein isothiocyanate (FITC) conjugate of Annexin-V (a Ca-dependent phospholipid-binding protein with high affinity for PS) is used allowing detection of apoptosis. Since membrane permeabilisation is observed in necrosis, necrotic cells will also bind Annexin-V−FITC. PI is used to distinguish between viable, early apoptotic and necrotic or late apoptotic cells. Necrotic cells bind Annexin-V−FITC and stain with PI, while PI is excluded from viable (FITC negative) and early apoptotic (FITC positive) cells. In the absence of phagocytosis final stages of apoptosis involve necrotic-like disintegration of the total cell, thus cells in late apoptosis will be labeled with both FITC and PI. Fluorescence of PI (FL3) is plotted versus Annexin-V fluorescence (FL1) as shown in Figure 6 for the positive controls and complex **4**. The early apoptosis in percentage were compared for the tested compounds (Figure S8). Elevated early apoptosis was observed for one of the studied ligand precursors (H_2L^2) and complexes **3** and **4** as well as for cisplatin and M627 compared with the DMSO control. According to these data the studied compounds can be considered as moderate apoptosis inducers. The percentage of the late apoptosis and necrosis gated events was found to be significantly higher for the metal free precursors (H_2L^1: 51.9%, H_2L^2: 68.7% *vs* complex **3**: 24.7% and **4**: 30.1%) at the applied concentration (20 μM).

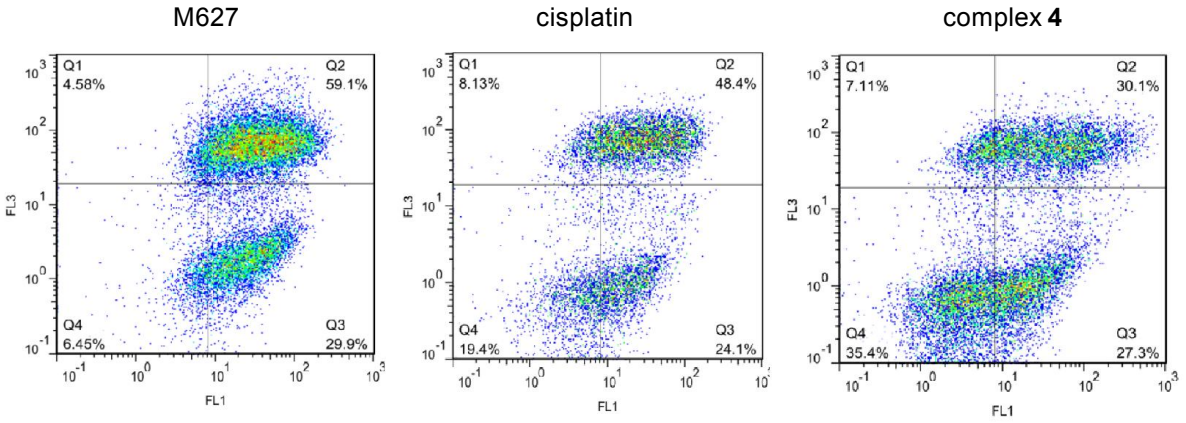

Figure 6. Quantification of apoptosis in cells treated with complex **4** and M627, cisplatin (as positive controls) using the Annexin-V/PI double staining assay. A549 cells were treated with 20 μM of compounds. The dual parametric dot plots combining Annexin-V (FL1) and PI (FL3) fluorescence show the viable cell population in the lower left quadrant Annexin-V^-/PI^- (Q4), the early apoptotic cells in the lower right quadrant Annexin-V^+/PI^- (Q3), and the late apoptotic cells in the upper right quadrant Annexin-V^+/PI^+ (Q2). (Number of cells counted: 19914 (M627), 9823 (cisplatin) 17166 (**4**).)

Conclusions

Two homologous optically active L-proline- and β^3-homoproline-thiosemicarbazone conjugates H_2L^1 and H_2L^2 were synthesized *via* multistep procedures. Substitution of the terminal amino group by pyrrolidine should presumably increase the lipophilicity, while insertion of one CH_2 group between the pyrrolidine moiety and COOH group of the amino acid enhanced the structural flexibility of the potential ligand. Both ligands were found to form square-planar complexes $[Ni(H_2L^1)Cl]Cl{\cdot}1.3H_2O$ (**1**$\cdot 1.3H_2O$), $[Pd(H_2L^1)Cl]Cl{\cdot}H_2O$ (**2**$\cdot H_2O$), $[Cu(H_2L^1)Cl]Cl{\cdot}0.7H_2O$ (**3**$\cdot 0.7H_2O$) and $[Cu(H_2L^2)Cl]Cl{\cdot}H_2O$ (**4**$\cdot H_2O$) by reactions of the ligands with the corresponding metal salts in ethanol or methanol. The two homologous ligand precursors and four metal complexes proved to be suitable for performing antiproliferative activity assays and establishment of notable and clear-cut structure-cytotoxicity relationships for three human cancer cell lines (A549, CH1 and SW480). The metal ions exert marked effects in a divergent manner: copper(II) modulates the cytotoxic potency of H_2L^1 and H_2L^2 in a beneficial way, whereas coordination to nickel(II) and palladium(II) impairs the antiproliferative activity of H_2L^1. The cytotoxicity of H_2L^1 and metal complexes **1**–**3** decreases in all three cell lines in the following rank order: **3** > H_2L^1 > **1** > **2**. Complex **3** exhibits the highest biological activity in all three cell lines with IC_{50} values of 2.4, 0.9 and 1.0 μM in A549, CH1 and SW480 cells, respectively. On the other hand compounds H_2L^1, H_2L^2, complexes **3** and **4** exhibited no tumor selectivity to cancerous cell lines over normal cells. The flow cytometry analysis of A549 cells stained for Annexin-V/PI showed induced early apoptosis in the case H_2L^2 and complexes **3** and **4**. The role of square-planar geometry in **1**–**3** (or more strictly in **2** and **3**) in the underlying mechanism of cytotoxicity seems to be negligible, while structural modifications at the terminal amino group of thiosemicarbazide and amino acid moiety have a significant impact on the

antiproliferative activity of both ligand precursors and copper(II) complexes. Substitution of the terminal NH_2 group of thiosemicarbazide moiety by pyrrolidinyl one resulted in 23- (in CH1 cells) and > 10-fold enhancement of cytotoxicity of metal-free compounds, and 5 to 5.5-fold increase for corresponding copper(II) complexes. In contrast, homologisation *via* insertion of a CH_2 group between pyrrolidine ring and carboxylate moiety of the amino acid, reduced markedly the cytotoxicity of the ligand and its copper(II) complex. The SARs found will be explored further for the development of effective anticancer agents in the discovered series of thiosemicarbazone-proline hybrids.

Supporting Information

Synthesis pathway to H_2L^2 (Scheme S1), ORTEP view of another crystallographically independent cation of **2** showing intermolecular hydrogen bonding interactions (Figure S1), fragments of the crystal structure of **1** and **2** revealing the intermolecular Pd···S contacts between two crystallographically independent cations (Figures S2 and S3), COSY ^1H–^1H NMR spectra of **2** (Figures S4 and S5), UV–vis spectra of H_2L^2 and **4** (Figures S6 and S7), hydrogen bonding interactions in **1** (Table S1) and selected matrix elements for simulation of ^1H NMR spectra of H_2L^1 and **2** (Table S2). Description of the assay for antiproliferative effect used to test the compounds in NIH/3T3 fibroblasts cell lines. Gated events (%) in the apoptosis assay obtained for the tested compounds (Figure S8).

AUTHOR INFORMATION

Corresponding Author

E-mail: vladimir.arion@univie.ac.at (V. B. A.)

Notes

The authors declare no competing financial interest.

ACKNOWLEDGMENTS

We are indebted to the Austrian Science Fund (FWF) for financial support of the project P28223-N34. We also thank Maria S. Novak and Dr. Michael Jakupec for performing the antiproliferative activity assays, Alexander Roller from the X-ray diffraction centre of the

Faculty of Chemistry of the University of Vienna for collection of X-ray data and Prof. Galanski for the measurement of NMR spectra.

References

(1) Thelander, L.; Gräslund, A. *J. Biol. Chem.* **1983**, *258*, 4063−4066.

(2) Yu, Y.; Kalinowski, D. C.; Kovacevic, Z.; Siafakas, A. R.; Jansson, P. J.; Stefani, C.; Lovejoy, D. B.; Sharpe, P. C.; Bernhardt, P. V.; Richardson, D. R. *J. Med. Chem.* **2009**, *52*, 5271−5294.

(3) Finch, R. A.; Liu, M.-C.; Cory, A. H.; Cory, J. G.; Sartorelli, A. C. *Adv. Enzyme Regul.* **2000**, *39*, 3−12.

(4) Traynor, A. M.; Lee, J. W.; Bayer, G. K.; Tate, J. M.; Thomas, S. P.; Mazurczak, M.; Graham, D. L.; Kolesar, J. M.; Schiller, J. H. A. *Invest. New Drug* **2010**, *28*, 91−97.

(5) Wadler, S.; Makower, D.; Clairmont, C.; Lambert, K.; Fehn, K.; Sznol, M. *J. Clin. Oncol.* **2004**, *22*, 1553−1563.

(6) Mackenzie, M. J.; Saltman, D.; Hirte, H.; Low, J.; Johnson, C.; Pond, G.; Moore, M. J. *Invest. New Drugs* **2007**, *25*, 553−558.

(7) Kolesar, J.; Brundage, R. C.; Pomplun, M.; Alberti, D.; Holen, K.; Traynor, A.; Ivy, P.; Wilding, G. *Cancer Chemother. Pharmacol.* **2011**, *67*, 393−400.

(8) (a) Karp, J. E.; Giles, F. J.; Gojo, I.; Morris, L.; Greer, J.; Johnson, B.; Thein, M.; Sznol, M.; Low, J. *Leuk. Res.* **2008**, *32*, 71−77; (b) Zeidner, J. F.; Karp, J. E.; Blackford, A. L.; Smith, B. D.; Gojo, I.; Gore, S. D.; Levis, M. J.; Garraway, H. E.; Greer, J. M.; Ivy, S. P.; Pratz, K. W.; McDevitt, M. A. *Haematologica* **2014**, *99*, 672–678.

(9) Jansson, P. J.; Kalinowski, D. S.; Lane, D. J.; Kovacevic, Z.; Seebacher, N. A.; Fouani, L.; Sahni, S.; Merlot, A. M. Richardson, D. R. *Pharmacol. Res.* **2015**, *100*, 255–260.

(10) Garcia-Tojal, J.; Gil-Garcia, R.; Gomez-Saiz, P.; Ugalde, M. *Curr. Inorg. Chem.* **2011**, *1*, 189–210.

(11) Yu, Y.; Kalinowski, D.S.; Kovacevic, Z.; Siafakas, A.R.; Jansson, P. J.; Stefani, C.; Lovejoy, D. B.; Sharpe, P. C.; Bernhardt, P. V.; Richardson, D. R. *J. Med. Chem.* **2009**, *52*, 5271−5294.

(12) Kalinowski, D. S.; Richardson, D. R. *Pharmacol. Rev.* **2005**, *57*, 547–583.

(13) Tisato, F.; Marzano, C.; Porchia, M.; Pellei, M.; Santini, C. *Med. Res. Rev.* **2010**, *30*, 708−749.

(14) Easmon, J.; Puerstinger, G.; Heinisch, G.; Roth, T.; Fiebig, H.H.; Holzer, W.; Jaeger, W.; Jenny, M.; Hofmann, J. *J. Med. Chem.* **2001**, *44*, 2164–2171.

(15) Zeglis, B. M.; Divilov, V.; Lewis, J. S. *J. Med. Chem.* **2011**, *54*, 2391−2398.

(16) Liu, M-C.; Lin, T.-S.; Sartorelli, A. C. *J. Med. Chem.* **1992**, *35*, 3612–3611.

(17) Li, J.; Niu, C-S.; Li, X.; Doyle, T. W.; Chen, S-H. *Patent U.S.* **1998**, US5767134 A 19980616.

(18) a) Sava, G.; Jaouen, G.; Hillard, E. A.; Bergamo, A. *Dalton Trans.* **2012**, *41*, 8226–8234; b) Hait, W. N. *Cancer Res.* **2009**, *69*, 1263–1267; c) Gasser, G.; Ott, I.; Metzler-Nolte, N. *J. Med. Chem.* **2011**, *54*, 3–25.

(19) Milunovic, M. N. M.; Enyedy, E. A.; Nagy, N. V.; Kiss, T.; Trondl, R.; Jakupec, M. A.; Keppler, B. K.; Krachler, R.; Novitchi, G.; Arion, V. B. *Inorg. Chem.* **2012**, *51*, 9309−9321.

(20) Maylonas, S., Mamalis, A. *J. Heterocyclic Chem.* **2005**, *42*, 1273−1281.

(21) Klayman, D. L.; Bartosevich, J. F.; Griffin, T. S.; Mason, C. J.; Scovill, J. P. *J. Med. Chem.* **1979**, *22*, 855–862.

(22) (a) Wang, Q.; Wilson, C.; Blake, J. A.; Collinson, R. S.; Tasker, A. P.; Schröder, M. *Tetrahedron Lett.* **2006**, *47*, 8983−8987; (b) Huisman, M.; Koval, I. A.; Gamez, P.; Reedijk, J. *Inorg. Chim. Acta* **2006,** *359*, 1786−1794.

(23) Corey, E. J.; Shibata, S.; Bakshi, R. K. *J. Org. Chem.* **1988**, *53*, 2861–2863.

(24) Cassal, J.-M.; Fürst, A.; Meier, W. *Helv. Chim. Acta* **1976**, *59*, 1917–1924.

(25) *SAINT-Plus*, version 7.06a and APEX2; Bruker-Nonius AXS Inc.: Madison, WI, 2004;

(26) Sheldrick, G. M., *Acta Crystallogr.* **2008**, *A46*, 112–122.

(27) Johnson, G. K. Report ORNL-5138; OAK Ridge National Laboratory; Oak Ridge, TN, 1976.

(28) Mucsi, I.; Varga, A.; Kawase, M.; Motohashi, N.; Molnar, J. *Anticancer Res.* **2002**, *22*, 2833–2836.

(29) Arndt, F.; Eistert, B. "Ein Verfahren zur Überführung von Carbonsäuren in ihre hö-heren Homologen bzw. deren Derivate" *Ber. Dtsch. Chem. Ges.* **1935**, *68*, 200−208.

(30) (a) Sunkel, K.; Hoffmuller, W.; Beck, W. *Z. Naturforsch.* **1998**, *53b*, 1365–1368; (b) Poth, T.; Paulus, H.; Elias, H.; Dücker-Benfer, C.; van Eldik, R. *Eur. J. Inorg. Chem.* **2001**, 1361–1369; (c) Yousef, R. I.; Bette, M.; Kaluderović, G. N.; Paschke, R.; Yiran, C.; Steinborn, D.; Schmidt, H. *Polyhedron* **2011**, *30*, 1990–1996; (d) Carmona, D.; Lahoz, F. J.; Atencio, R.; Oro, L. A.; Lamata, M. P.; Viguri, F.; José, E. S.; Vega, C.; Reyes, J.; Joó, F.; Kathó, Á. *Chem. Eur. J.* **1999**, *5*, 1544–1564.

(31) (a) Carmona, D.; Lamata, M. P.; Viguri, F.; Dobrinovich, I.; Lahoz, F. L.; Oro, L. A. *Adv. Synth. Catal.* **2002**, *344*, 499–502; (b) Bacher, F.; Enyedy, É. A.; Nagy, N. V.; Rockenbauer, A.; Bognár, G. M.; Trondl, R.; Novak, M. S.; Klapproth, E.; Kiss, T.; Arion, V. B. *Inorg. Chem.* **2013**, *52*, 8895−8908.
(32) Kovala-Demertzi, D.; Yadav, P. N.; Demertzis, M. A.; Jasiski, J. P.; Andreadaki, F. J.; Kostas, I. D. *Tetrahedron Lett.* **2004**, *45*, 2923−2926.
(33) Addison, A. W.; Rao, T. N.; Reedijk, J.; van Rijn, J.; Verschoor, G. C. *J. Chem. Soc. Dalton Trans.* **1984**, 1349–1356.
(34) Karplus, M. *J. Am. Chem. Soc.* **1963**, *85*, 2870–2871.
(35) Minch, M. J. Concepts in Magnetic Resonance, **1994**, *6*, 41–56.
(36) Cai, M.; Huang, Y.; Liu, J.; Krishnamoorthi, R. *J. Biomol. NMR* **1995**, *6*, 123–128.
(37) Abraham, R. J.; Hudson, B. D.; Thomas, W. A. *Magn. Res. Chem*. **1986**, *24*, 812–815.
(38) (a) Evans, D. F. *J. Chem. Soc.* **1959**, 2003–2005; (b) Sur, S. K. *J. Magn. Reson.* **1989**, *82*, 169–173.
(39) (a) O. Kahn, O. *Molecular Magnetism*, VCH Publishers, Inc., New York, Weinheim, Cambridge, 1993, 393 p.; b) R. Carlin, *Magnetochemistry*, Springer Verlag, 1986, 320 p.
(40) González, E.; Rodrigue-Witchel, A.; Reber, C. *Coord. Chem. Rev.* 2007, *251*, 351–363.
(41) (a) Robinson, M. A.; Curry, J. D.; Busch, D. H. *Inorg. Chem.* **1963**, *2*, 1178–1181; (b) Dobrov, A.; Arion, V.B.; Shova, S.; Roller, A.; Rentschler, E.; Keppler, B.K. *Eur. J. Inorg. Chem.* 2008, 4140–4145.
(42) Tanabe Y.; Sugano, S. *J. Phys. Soc. Jpn.* **1954**, *9*, 753–766.
(43) Lever, A. B. P. *Inorganic Electronic Spectroscopy*, 1968.
(44) Chellan, P.; Shunmoogam-Gounden, N.; Hendricks, D. T.; Gut, J.; Rosenthal, P. J.; Lategan, C.; Smith, P. J.; Chibale, K.; Smith, G. S. *Eur. J. Inorg. Chem.* **2010**, 3520–3528.
(44) Primik, M. F.; Mühlgassner, G.; Jakupec, M. A.; Zava, O.; Dyson, P. J.; Arion, V. B.; Keppler, B. K. *Inorg. Chem.* **2010**, *49*, 302−311.
(45) Pichler, V.; Valiahdi, S. M.; Jakupec, M. A.; Arion, V. B.; Galanski, M.; Keppler, B. K. *Dalton Trans.* **2011**, *40*, 8187–8192.

Graphical Abstract

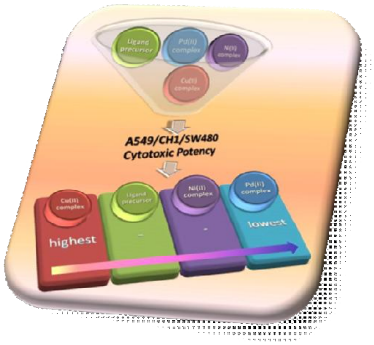

The *in vitro* anticancer potency of ligand precursors H_2L^1 and H_2L^2 and $[Ni(H_2L^1)Cl]Cl$ (**1**), $[Pd(H_2L^1)Cl]Cl$ (**2**), $[Cu(H_2L^1)Cl]Cl$ (**3**) and $[Ni(H_2L^2)Cl]Cl$ (**4**) was studied in three human cancer cell lines (A549, CH1 and SW480). Clear-cut structure-activity relationships have been established. The metal ions exert marked effects in a divergent manner: copper(II) increases, whereas nickel(II) and palladium(II) decrease the cytotoxicity of the hybrids. The antiproliferative activity of H_2L^1 and metal complexes **1**–**3** decreases in all three cell lines in the following rank order: **3** > H_2L^1 > **1** > **2**.